Electronic structure and transport properties of doped PbSe

Haowei Peng,[1,*] Jung-Hwan Song,[1] M. G. Kanatzidis,[2] and Arthur J. Freeman[1]
[1]*Department of Physics and Astronomy, Northwestern University, Evanston, Illinois 60208, USA*
[2]*Department of Chemistry, Northwestern University, Evanston, Illinois 60208, USA*
(Received 14 September 2010; revised manuscript received 8 August 2011; published 13 September 2011)

Understanding the electronic structure and transport properties of doped PbSe for its thermoelectric applications is an urgent need. Using a first-principles approach, we first explore the band structures of PbSe doped with a series of impurities, including cation-site substitutional impurities (Na, K, Rb; Mg, Ca, Sr; Cu, Ag, Au; Zn, Cd, Hg; Ga, In, Tl; Ge, Sn; As, Sb, Bi) and anion-site substitutional impurities (P, As, Sb; O, S, Te). Then we calculate the density of states (DOS) difference between the doped samples and pure host sample, which is a useful quantity to recognize the possibility of improving transport properties. The exhibited chemical trends and the nature of the impurity states are well explained with a simplified linear combination of atomic orbitals (LCAO) picture. Finally, we calculate the transport properties of these doped systems within the framework of Boltzmann theory and constant relaxation time approximation. Typical competing behavior between the electrical conductivity and Seebeck coefficient is exhibited, and a significant enhancement of thermoelectric power factor is found in the cation-site Au-doped p-type samples, and cation-site As-doped n-type samples.

DOI: 10.1103/PhysRevB.84.125207 PACS number(s): 71.20.Nr, 71.55.Ht, 72.15.Jf

I. INTRODUCTION

The performance of a material used in thermoelectric devices is characterized by a dimensionless figure of merit, $zT = S^2\sigma T/(\kappa_e + \kappa_l)$, where S is the Seebeck coefficient, σ is the electrical conductivity, T is the absolute temperature, and κ_e and κ_l are the electronic and lattice thermal conductivities.[1] Among these quantities, S, σ, and κ_e, which couple with each other, are mainly determined by the electronic structure, whereas κ_l is related to the lattice. In the past, most approaches to enhance the figure of merit managed to reduce the lattice thermal conductivity,[2,3] such as by using nanostructures, superlattice structures, skutterudite, and so on. However, the lattice thermal conductivity of semiconductors has a practical lower limit which occurs in the so-called phonon glass electron crystal.[4] Another way is to maximize the numerator of z, i.e., the power factor $S^2\sigma$. For a given material, one can optimize the power factor by varying the dopant concentration, thereby varying the carrier density.[5] From the perspective of material design, Mahan and Sofo[6] proposed that in the best thermoelectric materials the energy carriers should have a distribution in energy as narrow as possible but with high carrier velocity in the direction of the applied electric field. With respect to the electronic structure, a sharp increase in the density of states (DOS) near the Fermi level may be beneficial, which has been supported by recent theoretical and experimental studies.[7,8] In the theoretical work,[7] enhancement of the power factor is found in so-called highly mismatched alloys (HMAs), where highly electronegativity mismatched isoelectronic doping results in a sharp local increase of the DOS. In the experimental work,[8] it was reported that doping of 2% Tl in PbTe led to a doubling of the zT compared with the best conventional p-type PbTe alloy, PbTe:Na. According to the theory of Mahan and Sofo,[6] this enhancement should be related to the Tl-induced resonance states in the valence band which results in a local increase of the density of states (DOS) near the Fermi level.

PbTe-based materials,[3,9,10] including nanostructures, alloys, and also the 2% Tl-doped bulk materials,[8] have shown good properties in thermoelectric applications. Compared with PbTe, another lead chalcogenide, PbSe has several advantages with respect to thermoelectric application. First of all, selenium is much more abundant than tellurium, which can reduce the cost of related devices. Second, bulk PbSe has a smaller lattice thermal conductivity than PbTe,[11] which is beneficial for a larger figure of merit. Third, bulk PbSe has a higher melting temperature than PbTe (1082 °C versus 924 °C),[12] which means a possibly better thermal stability. In this study, we investigate the electronic structures and transport properties of PbSe doped with a serial of impurities including cation-site substitutional impurities (Na, K, Rb; Mg, Ca, Sr; Cu, Ag, Au; Zn, Cd, Hg; Ga, In, Tl; Ge, Sn; As, Sb, Bi) and anion-site substitutional impurities (P, As, Sb; O, S, Te), using first-principles band structure calculations. We calculate the difference between the DOS of the doped samples and the pure host sample to find a local increase near the Fermi level. A similar calculation on PbTe was performed in a previous study,[13] which will be compared here. The chemical trends and the nature of impurity states are well described using the linear combination of atomic orbitals (LCAO) picture. Within the framework of Boltzmann theory,[14] using the constant relaxation time approximation and rigid band model, the transport properties and the power factor for the semiconducting doped samples are calculated. We find that (1) changes in the DOS of PbSe due to different impurities are very similar with those that happen to PbTe; (2) there is a significant enhancement of the power factor in cation-site Au- and As-doped PbSe; (3) with the impurity concentration in this work (3.125%), Tl doping does not improve the thermoelectric properties of PbSe; (4) the HMA method is not applicable for PbSe, so it is not universal.

The rest of this article is as follows. In Sec. II, we describe the calculation methods in detail. In Sec. III, the electronic structures of pure PbSe and doped PbSe are described, and the effects of doping on the electronic structure and transport properties are discussed. Based on these results, we summarize several general rules for PbSe in Sec. IV.

II. METHOD OF CALCULATION

The first-principles band structure calculations within the framework of density functional theory were based on the Perdew-Burke-Ernzerhof[15] generalized gradient approximation (GGA) and the projected augmented wave method[16,17] as implemented in the VASP code.[18,19] The energy cutoff for the plane-wave expansion was 300 eV. The lattice constant of PbSe was optimized by fitting the calculated total energies and volumes with the Murnaghan equation of state.[20] The GGA result is 6.216 Å, which lies within the typical error bar compared with the experimental result, 6.124 Å. The impurity was modeled using a 64-atom $2 \times 2 \times 2$ rocksalt structure cubic supercell with one Pb or Se atom replaced by an impurity atom. A Γ-centered $5 \times 5 \times 5$ Monkhorst-Pack[21] k mesh was chosen to sample the Brillouin zone of the 64-atom supercell. All structures were fully relaxed until the residual atomic forces were smaller than 0.01 eV/Å. To calculate the change of the DOS, we aligned the single-particle eigenvalues of the perfect host sample and the doped sample according to the 1s core level of the farthest atom away from the impurity.

The Seebeck coefficient and electrical conductivity, and then the power factor, were calculated using the BoltzTraP code[22] within the framework of Boltzmann transport theory. The constant relaxation time approximation and rigid band model were used in this package. We calculated the single-particle eigenvalues with a dense Γ-centered $23 \times 23 \times 23$ k mesh using VASP, which were fed into the BoltzTraP. The BoltzTraP can analytically represent these band energies with a smoothed Fourier interpolation, and then we obtain necessary derivatives such as electron velocities for transport property calculations.

In the experiments,[3,8] the Na- and I-doped samples are usually used as reference samples for p-type and n-type samples, respectively. Because we use the same constant relaxation time for all the samples in this study, the calculated change in the transport properties originates from the change in the band structures. However, the relaxation time should be determined considering all possible scattering mechanisms, including[23,24] scattering by the deformation potential of acoustic and optical phonons, polar scattering by optical phonons, scattering by the short-range deformation potential of defects, and scattering by the Coulomb potential of defects. In different samples, the relaxation time could be different, but a similar relaxation time should be expected in samples with similar scattering sources. Also, it is unfair to directly compare the doped samples and the pure sample since there are no perfect hole- or electron-carrier suppliers which do not disturb the electronic structure of the pure host. Hence, in this study, we choose PbSe:Na, PbSe:I, and PbSe as reference samples for p-type, n-type, and isovalent impurity doped samples, respectively.

In PbSe, spin-orbit coupling (SOC) is very strong due to the heavy Pb atom. We performed calculations for all the samples both with and without SOC included. We find that SOC mostly affects the conduction bands; however, for the impurity states in most doped samples, especially in the acceptor-doped samples, if we trace the atomic characteristics of these states, their energy positions with respect to the host valence band maximum and their band dispersions do not change significantly when SOC is included. Besides, we compared the band structures of PbSe, PbSe:Tl, PbSe:Hg, PbSe:Bi, and PbSe:O, where the SOC effect may be very significant, calculated with VASP where the PBE-GGA is used and SOC is not included, and with the FLAPW[26] method where the screened-exchange LDA (sX-LDA) scheme[25] is used to remedy the band gap problem when the SOC is included. These calculations confirmed that for the p-type samples, neglecting the SOC is quite safe in this study, which probably results from a well-balanced error cancellation; however for the n-type samples, although the trend should still be correct, a more careful investigation is necessary, especially when the impurity is a heavy element such as Bi. Hence, in the following sections, we will mainly show our computed results without SOC. In most cases the correct qualitative trend can be expected. When the SOC may affect the transport properties in a significant way, an explicit description is given.

III. RESULTS AND DISCUSSION

A. Electronic structure of pure PbSe host

The electronic structures of PbSe, as well as PbTe and PbS, have been extensively studied using first-principles calculations.[27–29] Before moving on to the doped samples, we first summarize the electronic structure of PbSe. In Fig. 1(a), we plot the GGA band structures of the PbSe face-centered-cubic (fcc) unit cell with and without SOC included. As shown in the figure, SOC strongly affects the conduction bands and the valence bands near the Γ point where the Pb-p states make a large contribution. The band gaps calculated with and without SOC included are 0.38 eV and −0.04 eV (here the change of the sign denotes the exchange of the atomic characteristic of the band edges). To avoid this "negative" band gap, in the following work we focus on the results calculated without SOC included as mentioned above. In the range from −1.5 to 1.5 eV, which is most important to the transport properties, the band structures with or without SOC are very similar except for SOC lowering the conduction bands. Hence, a qualitatively correct trend should be expected even if the SOC is not included when exploring the electronic structure and transport properties of doped PbSe.

In Fig. 1(b), we plot the l-decomposed site-projected DOS (PDOS) of PbSe without SOC included. As shown in the figure, the valence and conduction bands of PbSe are predominately composed of the bonding and antibonding states between the Pb and Se p orbitals. The Se-s bands are located at about −12.0 eV. The Pb-s bands are more highly located in energy at about −8 eV. Near the valence band maximum (VBM), there is a significant Pb-s contribution, and near the conduction band minimum (CBM), there is also a noticeable Se-s contribution.

The evolution of the band structure from atomic orbitals can be described with a linear combination of atomic orbitals (LCAO) picture,[30] as shown in Fig. 1(c). From stage (I) to (II), only the Pb-p and Se-p interaction is considered. During this step, the main part of the conduction and valence bands are formed. We call the top valence states and bottom conduction states in stage (II) as VBM′ and CBM′ for convenience. From stage (II) to (III), the s-p interaction is turned on. The s-p interaction happens between the high-lying Pb-s and

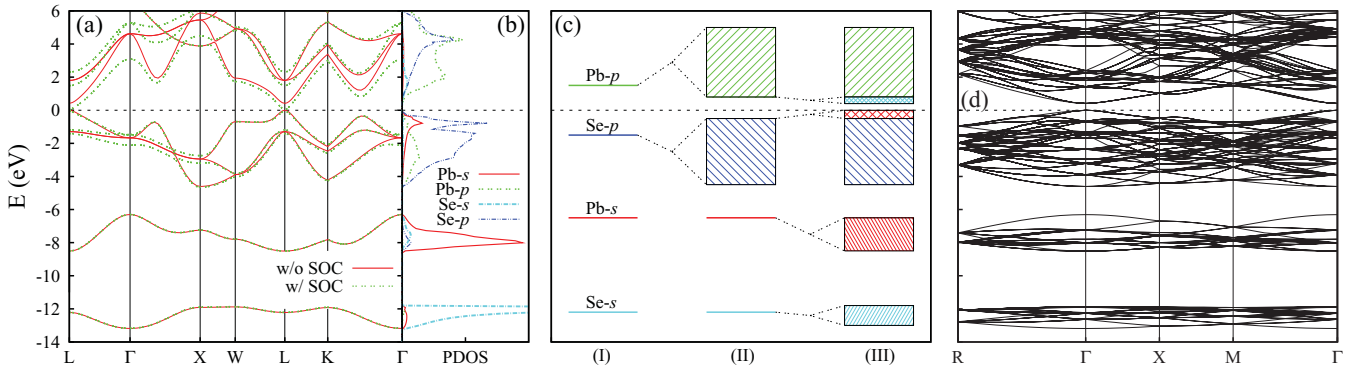

FIG. 1. (Color online) (a) Band structure of 2-atom fcc unit cell PbSe calculated with or without SOC included. (b) *l*-decomposed site-projected partial density of states (PDOS) of PbSe. (c) Simplified LCAO description of PbSe band structure: (I) the initial atomic states; (II) bands formed by including only the Pb-*p* and Se-*p* interaction; (III) the same as (II) but also including the Pb-Se *s*-*p* interaction. For clarity, we did not show the Pb-*s* and Se-*s* interaction. (d) Band structure of 64-atom cubic cell PbSe; SOC is not included. The energy zero is set at the valence band maximum.

VBM′ states, and also between the Se-*s* and CBM′ states. The former is much stronger because of the smaller energy distance between the Pb-*s* and VBM′ states, and both of them are especially strong near the *L* point because of the same symmetry.[27] The final top valence states at *L* consist of 42% Se-*p* and 22% Pb-*s* orbitals, whereas the top valence state at Γ consists of 48% Se-*p* and 0% Pb-*s* states, in the Wigner-Seitz spheres with radii of 3.26 and 2.20 bohrs for Pb and Se. This behavior leads to many peculiar electronic properties of PbSe. For example, the VBM occurs at *L* instead of at Γ,[31] and the band gap has a negative band gap deformation potential.[27,32] It is also the key to understand impurity states in group-III element doped samples. To obtain an intuitive picture for the effects of doping, we will employ this simplified LCAO model in combination with the first-principles method. In Table I in the Appendix, using a fully relativistic atomic code, we calculated the atomic orbital eigenvalues of the free atom for all the elements involved in this study, which can be used as parameters in the LCAO pictures.

Because the 64-atom supercell is used in impurity calculations, we plot in Fig. 1(d) the band structure of the 64-atom simple cubic supercell for PbSe. Compared with the 2-atom unit cell, the Brillouin zone (BZ) of the large supercell is reduced by a factor of 32. Four *L* points in the larger BZ fold into the Γ point in the smaller BZ,[33] so the direct band gap of the 64-atom cubic supercell happens at Γ and both the VBM and CBM states are fourfold degenerate, without considering spins. In most doped samples, the fourfold-degenerate states split into a triply degenerate state and a nondegenerate state. The triply degenerate states may have a higher or lower energy than the nondegenerate state, which is determined by the specific impurity.

From here on, we start to discuss the doped samples. At first, we show the results of Na- (and K-, Rb-) and I-doped samples, because they are used as reference samples for *p*- and *n*-type samples, respectively.

B. Na, K, and Rb substitution on the cation site

The alkali elements Na, K, and Rb have only one valence electron, and their valence *s* orbital is much higher in energy than Se-*p* and even Pb-*p* orbitals, as shown in Table I. Replacing a cation Pb in PbSe, Na, K, Rb will contribute the *s* electron to the valence band, introducing a hole. In experiments, Na is usually used to introduce holes into lead chalcogenides. As the ion size increases from Na to K to Rb, the impurity's nearest-neighbor Se [Se_1 in Fig. 3(a)] atoms relax outward from almost 0% in PbSe:Na to 2.7% in PbSe:K to 4% in PbSe:Rb. The band structures of PbSe:K with or without relaxation differ from each other in the dispersion of the impurity-related bands near the Fermi level and the splitting strength of the fourfold degenerate host VBM states, both of which are very important for the transport properties. Hence a full relaxation is necessary in such a study.

In Fig. 2, we compare the band structures and DOS of PbSe:X (X = Na, K, Rb) and PbSe host. There are two main changes in the band structures after doping. First is the splitting of the fourfold-degenerate VBM and CBM states into a set of high-energy triply degenerate states and a lower energy nondegenerate state. In the host PbSe, the VBM states are the antibonding states between the VBM′ (mainly Se-*p*) and Pb-*s* orbitals, with the former pushed upward by the latter [see Fig. 1(c)]. In PbSe:X (X = Na, K, Rb), a Pb-*s* orbital, which is below the VBM′ in energy, is replaced by an impurity-*s* which is high in the conduction band. As a result, one of the fourfold-degenerate host VBM states falls down due to the missing Pb-*s* orbital, and is further pushed down by the high impurity-*s* orbital. For the splitting of the host CBM states, a possible reason is the existence of impurity semicore *p* states, which push three of the host CBM states upward. These explanations are supported by the details: The splitting of the host VBM states decreases from PbSe:Na to PbSe:K to PbSe:Rb because the atomic eigenvalues of the impurity valence *s* orbitals shift upward from Na to Rb; and the splitting of the host CBM states increases from PbSe:Na to PbSe:K to PbSe:Rb, because the atomic eigenvalues of the impurity semicore *p* orbitals also shift upward from Na to Rb, as shown in Table I. The second change is that some flat bands appear, especially around the high-symmetry *k* points R, X, and M, and there are corresponding peaks for the increase in the DOS. As shown in Fig. 3(a), this mainly results from the hybridization

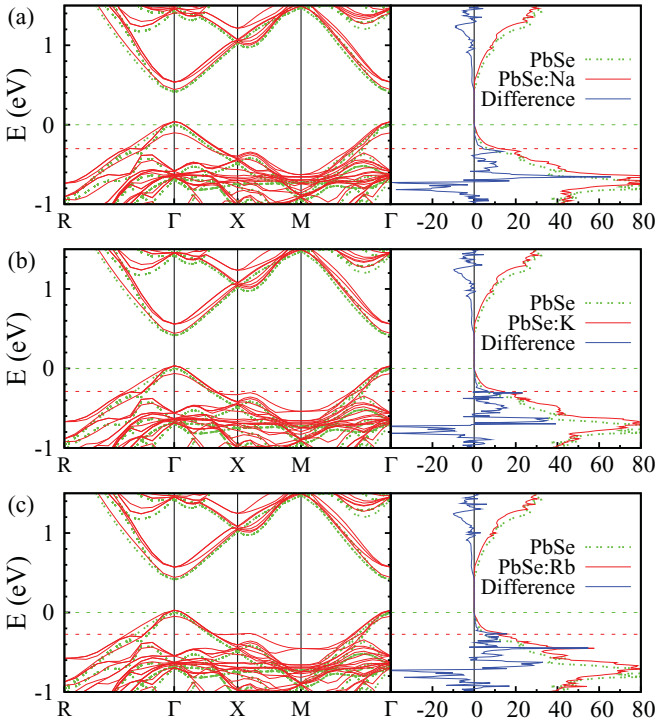

FIG. 2. (Color online) Band structures and densities of states (DOSs) of PbSe doped with (a) Na, (b) K, and (c) Rb. The eigenvalues are aligned between the doped samples and the pure host sample as explained in Sec. II. The horizontal dashed line at zero (green) denotes the VBM of pure PbSe, and the other (red) horizontal dashed line denotes the Fermi level in the doped sample. In the left panels, the band structures of doped samples and host PbSe are plotted using (red) solid lines and (green) double-dashed lines. In the right panels, the total DOSs of the doped samples and host PbSe are plotted with the same lines. Their difference is plotted with a (blue) thicker solid line: A positive value means an increase of DOS due to the doping.

between the impurity semicore p states and its nearest Se-p states.

In Figs. 3(b)–3(d), we plot the Seebeck coefficients, electrical conductivities, and power factors of PbSe:Na and PbSe:Rb as the carrier density changes. In this study, the impurity concentration is fixed at 3.125%. Given that the impurities are fully ionized, the carrier density should be about 0.033 e per unit cell. Using the rigid band model, we manually adjust E_F to change the population of the bands and the carrier density. According to the theory of Mahan and Sofo,[6] what is important for thermoelectric properties should be the increase of the DOS near E_F. A sharper peak in the DOS means a larger energy dependence of the DOS, which could lead to a larger Seebeck coefficient.[3,8] As shown in the right panels in Fig. 2, the increase of the DOS in PbSe:Rb is larger than that in PbSe:Na due to the localized states around the X point, and we find PbSe:Rb has a larger Seebeck coefficient in the low hole-carrier density condition, as shown in Fig. 3(b). Their electrical conductivities are comparable, as shown in Fig. 3(c), so we can obtain an enhanced power factor in PbSe:Rb compared with PbSe:Na, as shown in Fig. 3(d).

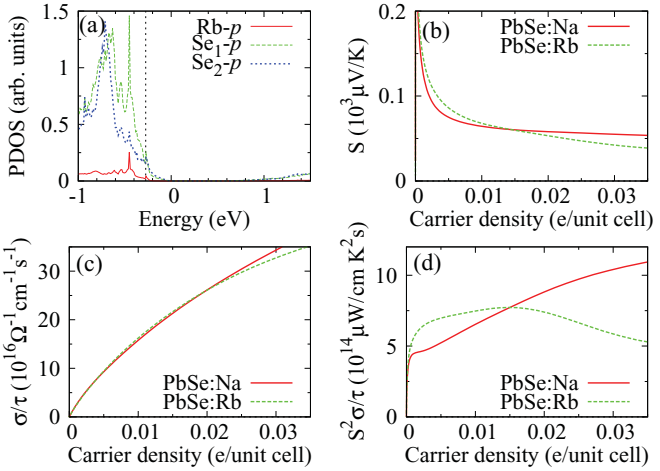

FIG. 3. (Color online) (a) PDOS plot for PbSe:Rb. Energy zero is set at the host VBM, and the vertical line denotes the Fermi level in the doped sample. Se_1 and Se_2 denote the nearest and farthest Se atom away from Rb in the 64-atom supercell, respectively. We can say that Se_1 is an impurity-related Se atom, while Se_2 is a kind of hostlike Se atom. (b) Seebeck coefficient, (c) electrical conductivity, and (d) power factor of PbSe:Rb at 300 K compared with PbSe:Na, all relative to the carrier density, where τ is relaxation time.

C. I substitution on the anion site

In Fig. 4, we compare the band structures and DOS of PbSe:I with that of pure PbSe. The change of the band structure mainly happens in the valence bands. As in PbSe:Na, the fourfold-degenerate VBM states also split into a set of triply degenerate states and a nondegenerate state. But now, because the I atom has lower p orbitals than Se, the triply degenerate states which mixed with some I-p states are located at lower energy. As shown in Fig. 5(a), the PDOS of I-p states is much lower in energy than that of the hostlike Se-p states. The conduction bands are almost not disturbed by replacing Se with I, and near the band edges there is no notable change in the DOS. In conclusion, substitutional I on the anion site acts as a perfect donor in PbSe, and, as expected, the Seebeck coefficient, electrical conductivity, and then the power factor of n-type PbSe:I are almost the same as that of n-type PbSe within the rigid band model, as shown in Figs. 5(b)–5(d).

In what follows, PbSe:I, PbSe:Na, and PbSe will be employed as reference samples for n-type, p-type, and isovalent impurity doped samples, respectively.

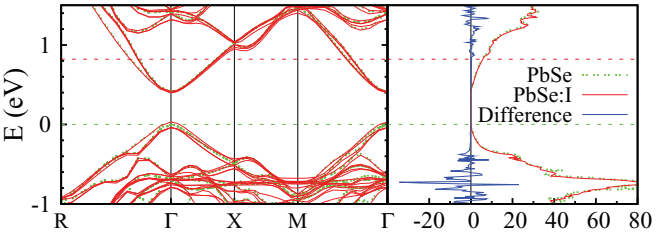

FIG. 4. (Color online) The same as in Fig. 2 but for PbSe:I with I doped on the anion site.

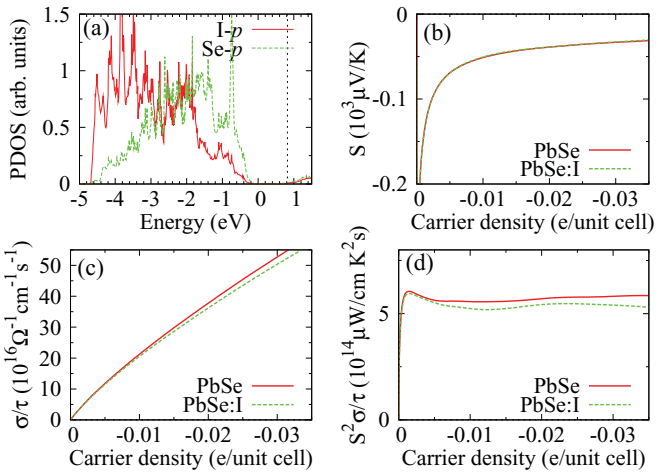

FIG. 5. (Color online) The same as in Fig. 3 but for PbSe:I with I doped on the anion site.

D. Mg, Ca, and Sr substitution on the cation site

In Fig. 6, we compare the band structures and DOS of PbSe:X (X = Mg, Ca, Sr) with pure PbSe. Now, Mg, Ca, and Sr have a valence configuration of p^6s^2 including the semicore p states. Since they are isovalent with Pb, doping Mg, Ca, and Sr does not introduce charge carriers, and there is almost no change of the VBM energy level compared to that of the undoped PbSe, as shown in Fig. 6.

It is easy to understand the electronic structure of Mg-, Ca-, and Sr-doped samples by comparing them with the Na-, K-, and Rb-doped samples, because all of them have an impurity s state lying high above the VBM, and semicore p states far below the VBM. But because the Mg-, Ca-, and Sr-s orbitals are closer to the VBM′ states than the corresponding Na-, K-, and Rb-s orbitals as listed in Table I, the splitting of the VBM states is larger in the Mg-, Ca-, and Sr-doped samples. Similarly, because the semicore p states of Mg, Ca, and Sr are much lower, the splitting in the CBM states is much smaller than that in the Na-, K-, and Rb-doped samples. For the same reason, the impurity–Se p-p interaction in alkali-doped samples is now negligible in the alkali-metal-doped samples. Correspondingly, there is no significant change in the DOS near the band edges, as shown in the right panels of Fig. 6.

Because the conduction band near the CBM is only slightly affected, the n-type PbSe:X (X = Mg, Ca, Sr) samples have similar transport properties with the PbSe host sample, or the PbSe:I sample. For the p-type samples, the Seebeck coefficient and electrical conductivity are comparable with PbSe:Na. Hence, it is possible to obtain a higher figure of merit by doping with Sr as a scattering center for phonons, which may decrease the lattice thermal conductivity without decreasing the power factor.

E. Cu, Ag, and Au substitution on the cation site

In Fig. 7, we compare the band structures and DOS of PbSe:X (X = Cu, Ag, Au) with PbSe. Now, Cu, Ag, and Au are also monovalent elements, as are Na, K, and Rb, so they act as acceptors. The differences are their much lower in energy valence s orbitals, and the presence of d orbitals which have comparable energies with the Se-p orbitals (Table I). The lower s orbitals introduce an impurity-s band near 1.2 eV. In PbSe:Au in Fig. 7(c), for example, if we trace the Au-s

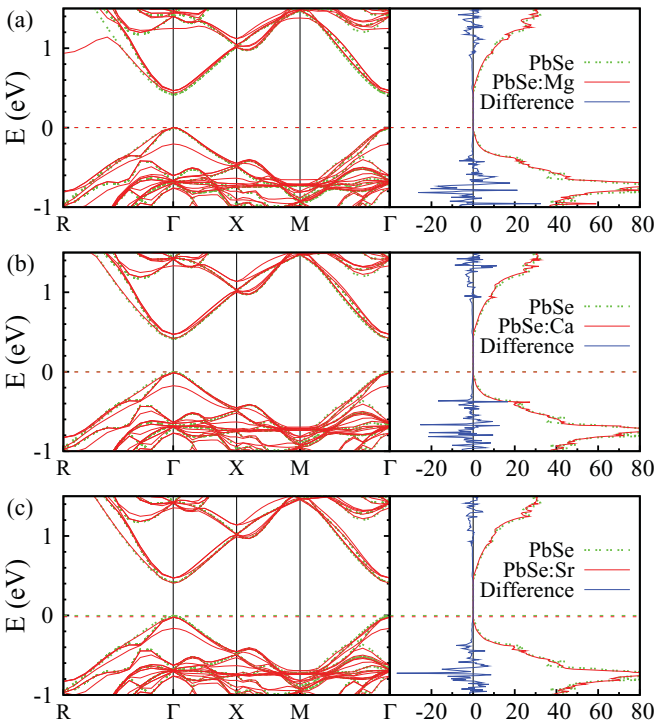

FIG. 6. (Color online) The same as in Fig. 2 but for (a) PbSe:Mg, (b) PbSe:Ca, and (c) PbSe:Sr.

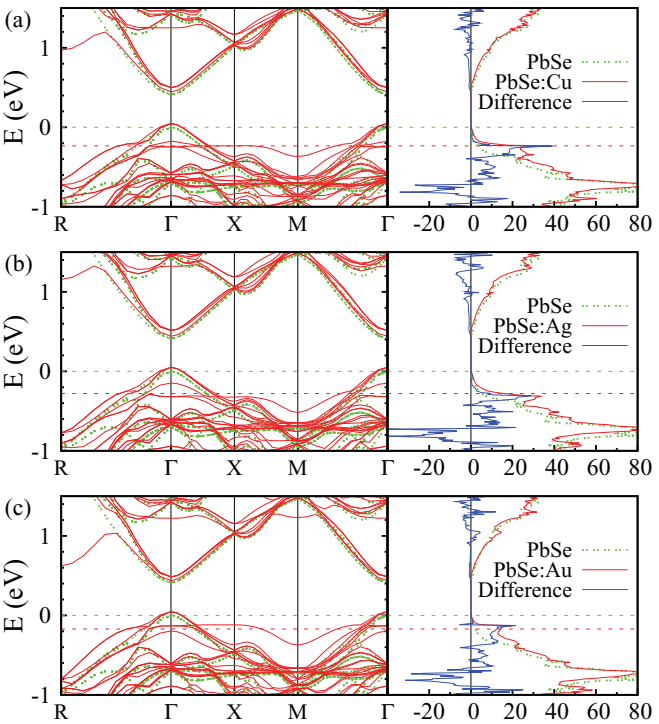

FIG. 7. (Color online) The same as in Fig. 2 but for (a) PbSe:Cu, (b) PbSe:Ag, and (c) PbSe:Au.

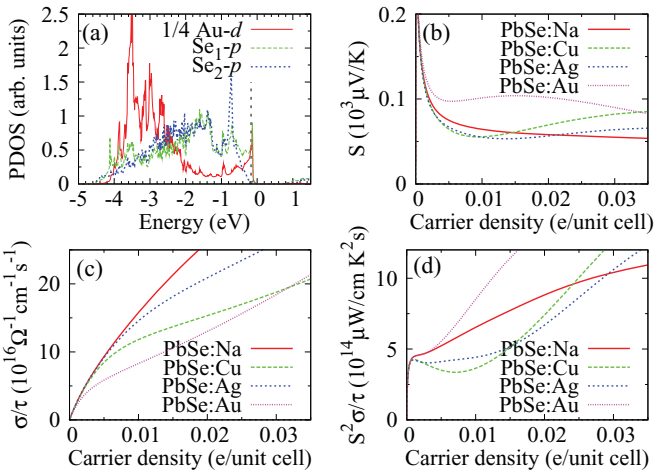

FIG. 8. (Color online) The same as in Fig. 3, but (a) for PbSe:Au, (b)–(d) for PbSe:X (X = Cu, Ag, Au).

contribution to the bands, we can find a flat s band which is located at around 1.2 eV from Γ to X to M to Γ. The effects of the impurity-d states are more significant: They form a very localized d band near E_F and lead to a very sharp increase of the DOS in all three samples, as shown in Fig. 7.

In Fig. 8(a), we plot the PDOS of Au-d, the impurity-related Se_1-p, and the hostlike Se_2-p states in PbSe:Au. In the rocksalt structure, the fivefold-degenerate d orbitals should split into a set of lower energy triply degenerate T_1^d states (d_{xy}, d_{yz}, d_{xz}) and a set of higher energy doubly degenerate E^d states (d_{z^2} and $d_{x^2-y^2}$), due to the octahedral crystal field splitting. The impurity T_1^d states can only couple weakly with Se-p states via π bonding, while the impurity E^d states couple with Se-p states via much stronger σ bonding. In Cu-, Ag-, and Au-doped PbSe, we found that the σ bonding is so strong that the impurity E^d states are pushed below the T_1^d states. In Fig. 8(a), the bonding states between Au E^d and Se p are located around −4 eV; the Au T_1^d states are mainly located between −4 and −2 eV; and the antibonding states between Au E^d and Se p are located at about the Fermi level. The impurity d PDOS in PbSe:Ag and PbSe:Au is very similar. In the Cu d PDOS plot of PbSe:Cu, three peaks are clearly separated: They are located at around −2.0, −1.0, and 0.0 eV corresponding to the E^d-related bonding states, T_1^d-related states, and E^d-related antibonding states, respectively. For the antibonding state, there is a 15%–36% contribution from the impurity E^d orbitals; thus the impurity band is very flat, as shown in Fig. 7 and mentioned above.

In Figs. 8(b)–8(d), we plot the Seebeck coefficients, electronic conductivities, and power factors for all three samples compared with the reference PbSe:Na sample. The hole concentration range in Figs. 8(b)–8(d) corresponding to the Fermi level moves from the top of the triply degenerate state (split from the fourfold-degenerate VBM) to the Fermi level denoted with a horizontal dashed line (red) in Fig. 7. In this range, a quite typical behavior is shown: The degree of localization of the impurity state or resonance state increases from PbSe:Ag to PbSe:Au to PbSe:Cu, as shown in Fig. 7; correspondingly, the Seebeck coefficient increases in the same sequence, whereas the electrical conductivity decreases in this sequence. Finally, we find in PbSe:Au a significant enhancement of the power factor as a result of such a competition. As shown in the plots, the Seebeck coefficient is almost doubled by doping 3.125% Au. The largest enhancement of the power factor happens at a hole-carrier concentration of about 0.028 e per unit cell, where the power factor is increased by 50% compared with PbSe:Na.

F. Zn, Cd, and Hg substitution on the cation site

Next to Cu, Ag, and Au in the periodic table are Zn, Cd, and Hg. There are three big differences between these two series. First, Zn, Cd, and Hg are divalent elements, so they will not introduce holes. As a result, the VBMs are almost at the same energy as the undoped host sample, similar to the alkali-metal-doped samples. Second, their d orbitals are more than about 0.3 Ry lower than those of Cu, Ag, and Au, respectively, as shown in Table I. Thus, the impurity d bands are located in the range of Pb-s bands, and they hardly affect the electronic structure near the band edge and then transport properties. The third is that the valence s orbitals in Zn, Cd, and Hg are much lower in energy than the corresponding Cu, Ag, and Au valence s orbitals. This has mainly two effects: One is that the splitting of the fourfold-degenerate VBM states is much stronger; the other, which is more important, is that there is a resonance state with an apparent impurity-s characteristic above the CBM, as shown in Fig. 9. From the Zn- to Cd- to Hg-doped samples, the energy position of the impurity-s band first increases then decreases. This behavior is in agreement with the atomic eigenvalues of Zn-, Cd-, and Hg-s orbitals listed in Table I. As shown in the table, the Hg-s is actually

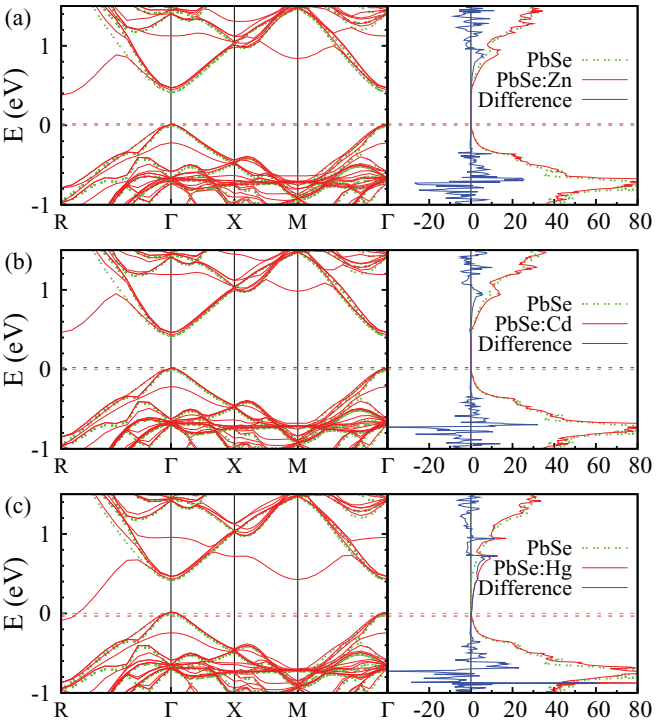

FIG. 9. (Color online) The same as in Fig. 2 but for (a) PbSe:Zn, (b) PbSe:Cd, and (c) PbSe:Hg.

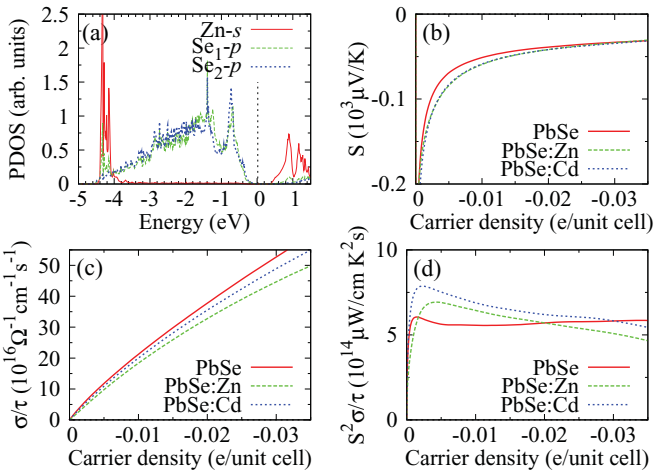

FIG. 10. (Color online) The same as in Fig. 3, but (a) for PbSe:Zn, (b)–(d) for PbSe:X (X = Zn, Cd).

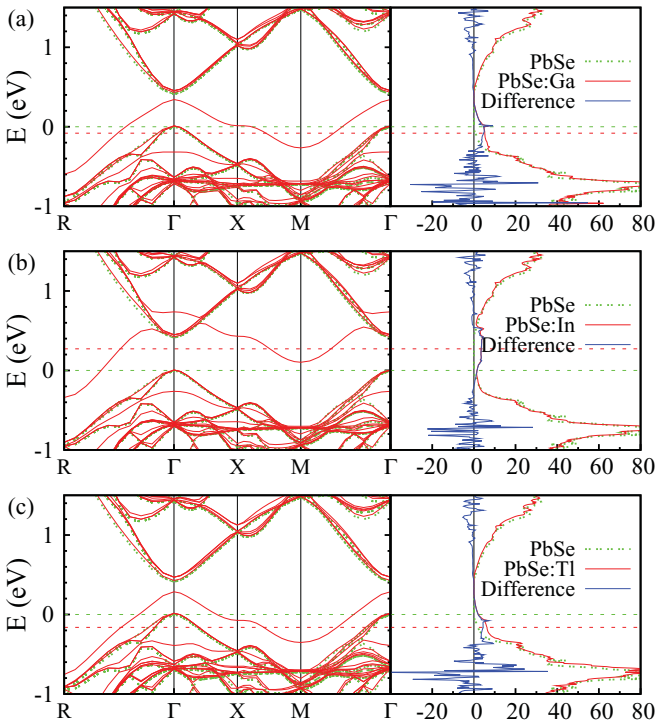

FIG. 11. (Color online) The same as in Fig. 2 but for (a) PbSe:Ga, (b) PbSe:In, and (c) PbSe:Tl.

lower than the Se-p orbital, which should be the reason why PbSe:Hg is a metal instead of a semiconductor, as is implicit in its band structure. Now if we focus on this resonance band, we find that the shape of this band resembles the shape of the top valence band. This is because although the resonance band is mainly composed of impurity-s and Pb-p orbitals, there are also contributions from the Se-p orbital. Hence, the impurity band has characteristics of an antibonding state formed by the impurity-s and Se-p orbitals, with the s orbital above the p orbital. As discussed above, the top valence band of PbSe is mainly the antibonding state formed by the Pb-s and Se-p orbitals but with the s orbital below the p orbital. So, where the Se-p is pushed upward strongly by the Pb-s, the impurity-s must also be pushed up strongly but by the Se-p. On the contrary, the impurity-s band has a minimum energy at R, where the Se-p does not hybridize strongly with the Pb-s. In the PDOS plot [Fig. 10(a)], the bonding state and the antibonding state between the Zn-s and its nearest Se_1-p states are clearly shown.

In Figs. 10(b)–10(d), we plot the Seebeck coefficients, electrical conductivities, and power factors of PbSe:Zn and PbSe:Cd, compared with host PbSe in the n-type range. Because PbSe:Hg is no longer a semiconductor, we did not consider this sample in the transport properties calculations. The Zn- and Cd-doped samples have similar Seebeck coefficients which are larger (in absolute value) than that of the host PbSe. The electrical conductivity of PbSe:Cd is slightly larger than that of PbSe:Zn, but slightly smaller than the pure host. As a result, we find an enhancement in both these samples, but PbSe:Cd seems better than PbSe:Zn. The enhancement could arise from two effects: One is the increase of the DOS due to the resonance state, but this should be an indirect origin because the local increase of the DOS lies too high in the conduction band; the other is the appearance of a new energy pocket which is formed by the resonance state near the high-symmetry k point R, as shown in Fig. 9.

Because the energy position of the impurity band at the special k point R is of particular importance, we have to consider the effects of SOC. The impurity band has the lowest energy at R, and the impurity states around R are more impurity-s-like. We know that the SOC would affect and shift down the Pb-p-like states. Thus when SOC is included, the impurity states around R will not shift down as much as other conduction bands because they are less Pb-p-like. In fact, in the calculations with SOC included, the impurity bands in PbSe:Zn and PbSe:Cd at R are 0.25 and 0.35 eV higher than the host CBM. The efficiency of the additional valley or energy pocket should decrease after the SOC is included. Hence the enhancement of the thermoelectric properties in PbSe:Zn and PbSe:Cd needs a more delicate investigation.

G. Ga, In, and Tl substitution on the cation site

Group-III elements Ga-, In-, and Tl-doped PbSe, PbTe, and PbS have been intensively studied both experimentally and theoretically, especially for PbTe.[13,33–36] Here we focus on PbSe samples, and compare our results with previous studies on PbTe samples. In Fig. 11, we plot the band structures and DOS of PbSe doped with Ga, In, and Tl. In all three samples, there is an impurity-related band which is totally detached from the remaining valence bands. Take PbSe:Tl for example; in Fig. 12, we compare the PDOS of Tl-s states, the hostlike (farthest away from Tl) Pb-s states, Tl-related Se_1-p states, and hostlike Se_2-p states. The PDOS plot shows that the impurity band shown in Fig. 11 is mainly the antibonding state between the Tl-s and its nearest neighboring Se-p orbitals. In previous studies[33,34] on Ga-, In-, and Tl-doped PbTe, the bonding state below the upper valence band was called the "hyperdeep defect state" (HDS), while the antibonding state near the VBM was called the "deep defect state" (DDS). In experiments,

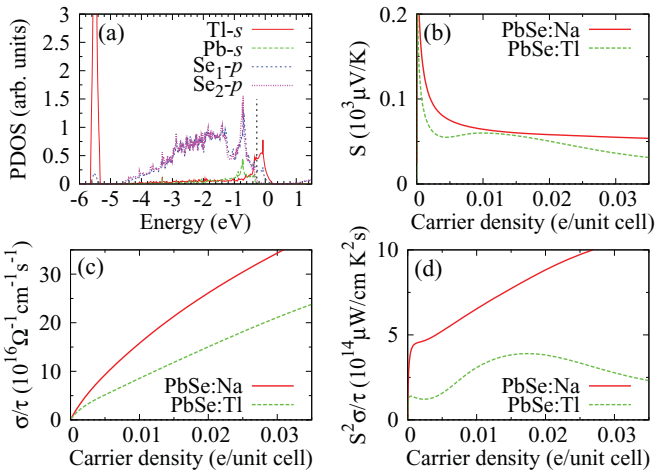

FIG. 12. (Color online) The same as in Fig. 3, but for PbSe:Tl.

the antibonding state was recognized[36] as a resonance state which results in significant enhancement of the thermoelectric properties in Tl-doped PbTe.[8] However, as shown in Fig. 11, the impurity band (or the DDS band) not only resonates in the valence band, but also largely extends into the band gap. In PbSe:In, this band even penetrates into the conduction band.

Interestingly, the energy position of the impurity band near the band edge is not monotonically increasing from the Ga- to In- to Tl-doped samples. For the corresponding PbTe samples,[33] this is explained by the strongest scalar relativistic effect[37] in Tl. Because Tl is the heaviest atom among Ga, In, and Tl, the core electrons of Tl have a smaller radius and lower energy due to the strongest relativistic effect. Then, the outer shell electrons, including the valence *s* electrons, will also have a reduced radius and a lower energy because of the orthogonality requirement. Thus, the valence *s* of Tl has the lowest energy as shown in Table I. Our calculations show that the valence *s* of Ga, In, and Tl have energies of −0.677, −0.621, −0.697 Ry, respectively. Then, with the same anion and the similar distance between the impurity and Se atoms, the energy position of the antibonding state should follow their atomic eigenvalues, which has been clearly shown in Fig. 11.

Here, we need to talk a little more about the effect of SOC in PbSe:In, because this is related to the position of the In-related impurity band. A good starting point is the band structures of the Zn-, Cd-, and Hg-doped samples. Here we ignore the SOC splitting; the band structures of the Zn-, Cd-, and Hg-doped samples can be estimated by shifting down the entire conduction band including most of the impurity states. However, for the Ga-, In-, and Tl-doped samples, we should almost fix the impurity bands and the valence band, and shift down the other empty bands. This is because in the Ga-, In-, and Tl-doped samples, the impurity bands are derived from the valence bands on which SOC has small effects. After this kind of shift, we shall find that the In impurity band is mainly above the host CBM, so In behaves as a donor in PbSe. This is in agreement with experiments.[35]

In Figs. 12(b)–12(d), we compare the Seebeck coefficient, electrical conductivity, and power factor of PbSe:Tl with those of the *p*-type reference sample PbSe:Na. Surprisingly, we find that both the Seebeck coefficient and electrical conductivity of PbSe:Tl are worse than those of PbSe:Na, which should result from the extension of the resonance states into the band gap. In this case, although there is a local increase of the DOS, this small increase is useless for thermoelectric properties. Besides, we repeated these calculations on PbSe:Tl and PbSe:Na using a 216-atom supercell with one impurity atom (at a concentration of about 1%); here, the Tl impurity band is less dispersive, but it is still separate from the rest of the valence bands and follows the shape of the host valence band. This kind of an impurity band may be called a "perturbed host band."[38] For the transport properties, using the 216-atom supercell model does not change the trends. And in experiments, doping Tl into PbSe does not improve the thermoelectric properties.[39]

H. Ge and Sn substitution on the cation site

Ge and Sn are located in the same column as Pb in the periodic table of elements. They are isovalent with Pb, but compared with Mg, Ga, and Sr, their valence electrons are *p* electrons like Pb, instead of *s* electrons. From Table I, the valence *p* orbits of Ge, Sn, and Pb are almost the same, so the conduction bands are almost not changed after doping, as shown in Fig. 13. Similarly, because Ge-4*s* and Pb-5*s* orbitals have a very close energy, the valence band in PbSe:Ge only differs a little from the undoped sample. The change in valence band of PbSe:Sn is similar with what happens in PbSe:Tl. The higher Sn-*s* states push a band out from the host valence band, but this is not as significant as that in PbSe:Tl.

For the transport properties, in the *n*-type condition, both PbSe:Ge and PbSe:Sn are very similar with the host material. In the *p*-type condition, PbSe:Ge is still similar to the pure host, and PbSe:Sn is only slightly better than PbSe:Tl.

I. As, Sb, and Bi substitution on the cation site

P, As, Sb, and Bi are group-V elements with five valence electrons. They can be donors or acceptors in PbSe, as determined by the cation or anion they substitute for. In

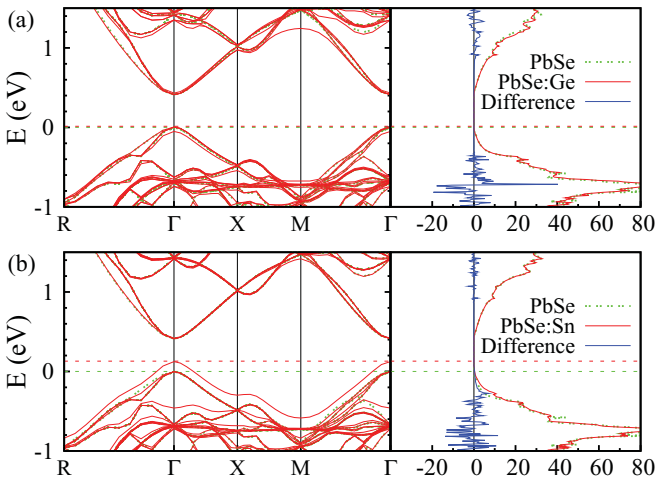

FIG. 13. (Color online) The same as in Fig. 2 but for (a) PbSe:Ge and (b) PbSe:Sn.

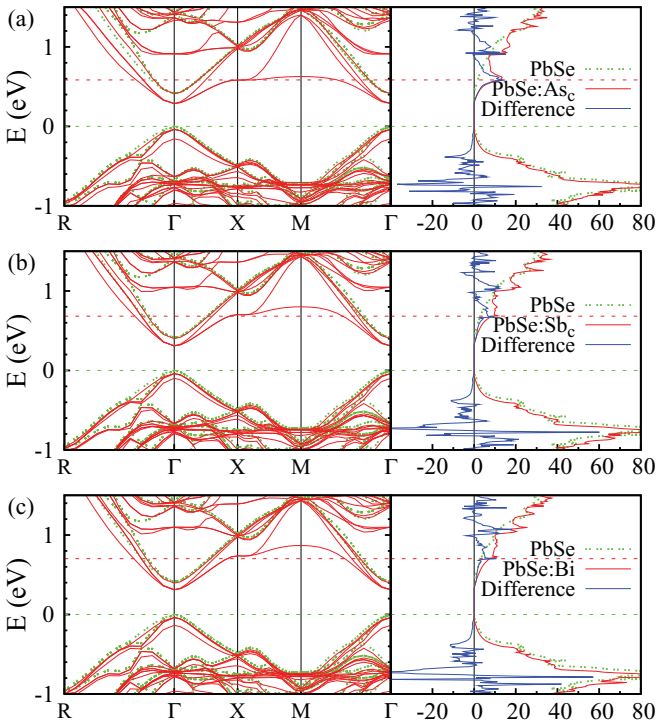

FIG. 14. (Color online) The same as in Fig. 2 but for (a) PbSe:As$_c$, (b) PbSe:Sb$_c$, and (c) PbSe:Bi.

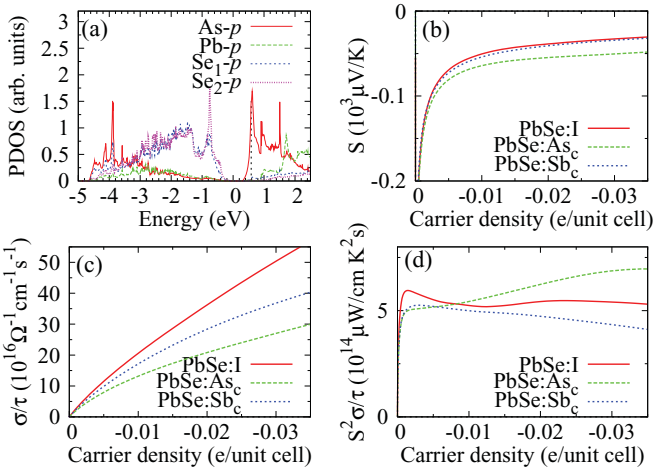

FIG. 15. (Color online) The same as in Fig. 3, but (a) for PbSe:As$_c$, (b)–(d) for PbSe:As$_c$, PbSe:Sb$_c$, and the reference sample PbSe:I.

this study, we consider As (As$_c$), Sb (Sb$_c$), Bi doped on the cation site, and P, As (As$_a$), Sb (Sb$_a$) doped on the anion site.

In Fig. 14, we compare the band structures and DOS of PbSe:X (X = As$_c$, Sb$_c$, Bi) with PbSe. The most significant change, after doping, occurs in the conduction band. Because the impurity valence p are lower than the Pb-p, some bands are pulled down by the negative impurity potential. Related effects include the splitting of the original fourfold-degenerate CBM states into a set of lower energy triply degenerate states and a high-energy nondegenerate state, the appearance of resonance states near 1 eV, and the more important flat band near the Fermi level. The latter two are the origin of the local increase of the DOS as shown in the right panels in Fig. 14. In Fig. 15(a), we compare the PDOS of As-p and hostlike Pb-p, and As-related Se$_1$-p and hostlike Se$_2$-p states in PbSe:As$_c$. The As-p and Se$_1$-p states form antibonding (bonding) states in the bottom of the conduction band (upper valence band). The valence band is changed in a way similar to that in PbSe:Tl, but in PbSe:Tl the bands are shifted upward because the Tl-s orbital is higher than the Pb-s, whereas in PbSe:X (X = As$_c$, Sb$_c$, Bi) some bands are shifted downward. This is also reflected by the decrease of the DOS below the host VBM, as shown in Fig. 14.

We calculated the transport properties for all three samples. In Figs. 15(b)–15(d), we present the results for As$_c$- and Sb$_c$-doped samples, compared with the n-type reference PbSe:I sample. The transport properties of PbSe:Bi are very similar to those of PbSe:Sb$_c$. Now, PbSe:As$_c$ has a better Seebeck coefficient and a poorer electrical conductivity than PbSe:Sb$_c$, as a result of the little more localized impurity band near the Fermi energy. But the gain from the Seebeck coefficient leads to an enhanced power factor due to the squared relationship.

However, in these n-type samples, the spin-orbit coupling may change the conclusion. The most important change after including the SOC is that the doubly degenerate flat band near the X point in Fig. 14 and the flat band along X-M-Γ become slightly more dispersive. These should reduce the Seebeck coefficient, and also increase the electrical conductivity. Thus a more detailed investigation is necessary.

J. P, As, and Sb substitution on the anion site

When the group-V elements replace the anion in PbSe, they act as acceptors. In Fig. 16, we plot the band structures and DOS of PbSe:P, PbSe:As$_a$, and PbSe:Sb$_a$. The difference with the previous cases is that the triply degenerate states are below the nondegenerate state for both the VBM and CBM states. This is because the impurity-s and impurity-p are higher in energy than the Se-s and Se-p, respectively. Recalling the contribution of the anion s to the host CBM as shown in Fig. 1, the higher impurity-s orbital raises one of the fourfold-degenerate CBM states; similarly, the higher impurity-p states raise three of the fourfold-degenerate VBM states. The splitting of the CBM states increases from As$_a$- to P- to Sb$_a$-doped samples, in agreement with the increase of the valence s atomic eigenvalues from As to P to Sb. Also, the splitting of the VBM increases in the same way as the valence p atomic orbital eigenvalues of these three impurity atoms.

The changes in the valence band of PbSe:X (X = P, As$_a$, Sb$_a$) are a little symmetrical with the changes in the conduction band of PbSe:X (X = As$_c$, Sb$_c$, Bi). Resonance arising from the impurity-p state, and a flat impurity band near E_F, also appears in the anion-site-doped samples. This is because both the conduction band and valence band of PbSe mainly consist of p atomic orbitals. But, at the top of the valence band of PbSe, there is a significant s-p interaction between the cation and anion. In Fig. 17(a), we plot the PDOS of Sb-p, hostlike

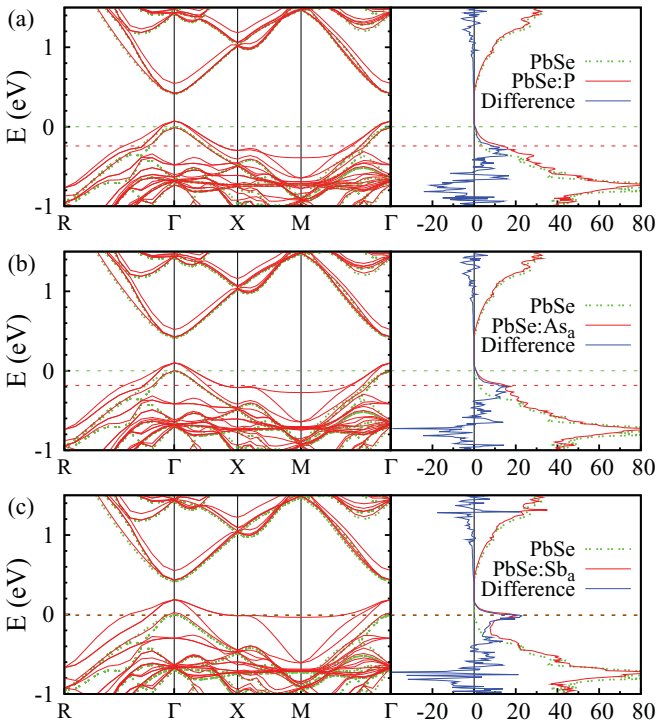

FIG. 16. (Color online) The same as in Fig. 2 but for (a) PbSe:P, (b) PbSe:As$_a$, and (c) PbSe:Sb$_a$.

Se-p, impurity-related Pb$_1$-s, and hostlike Pb$_2$-s in PbSe:Sb$_a$. The upward shift of the impurity-related Pb$_1$-s PDOS due to the Sb-p is clearly seen.

Considering the width of the PbSe upper valence band, the position of the impurity-p atomic orbitals should be located in the top part of the valence band. These impurity-p orbitals lead to a significant local increase of the DOS near E_F as shown in the right-hand panels in Fig. 16. As the impurity valence p increases from P to As to Sb, the increase of the DOS, and then E_F, shifts upward. In PbSe:Sb$_a$, E_F is pinned near the host VBM because of the very flat impurity band. Although the impurity band also extends into the band gap, the big increase in the DOS should lead to a huge enhancement of the Seebeck coefficient, and also to a significantly reduced electrical conductivity.

In Figs. 17(b)–17(d), the transport properties of PbSe:As$_a$ and PbSe:Sb$_a$ are compared with the reference sample PbSe:Na. As analyzed above, only a slight enhancement of the power factor is found when the hole concentration is low. In the PbSe:P sample, the bands are more dispersive; as a result, the electronic conductivity is a little larger than that of PbSe:As$_a$, but the Seebeck coefficient is not increased any more. In PbSe:P, we did not find an enhancement in the power factor.

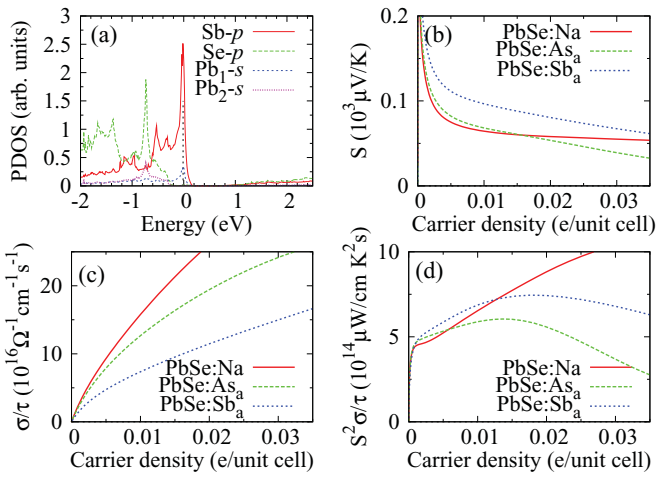

FIG. 17. (Color online) The same as in Fig. 3, but (a) for PbSe:Sb$_a$, (b)–(d) for PbSe:Sb$_a$, and the reference sample PbSe:Na. In (a), Se denotes the hostlike Se atom which is farthest away from Sb. Pb$_1$ denotes the impurity's nearest neighboring Pb atom, and Pb$_2$ denotes the hostlike Pb atom which is farthest away from Sb.

K. O, S, and Te substitution on the anion site

O, S, and Te are in the same column of the periodic table of elements as Se. As shown in Table I, their valence atomic orbitals gradually shift upward from the top to the bottom of this column. Among these, the O valence s and p orbitals are far lower than those of the other three, especially the valence s. In Fig. 18, we compare the band structures and DOS of O-, S-, and Te-doped samples with the pure host sample. Generally speaking,[40] if the impurity atom is more electronegative than the replaced atom, the bands will be dropped down by the impurity-related attractive potential; otherwise the bands will be pushed up by the repulsive potential. The electronegativity difference or the impurity-related potential can be estimated from the energy difference of the valence atomic orbitals:[41] O is much more electronegative than Se, so the bands are

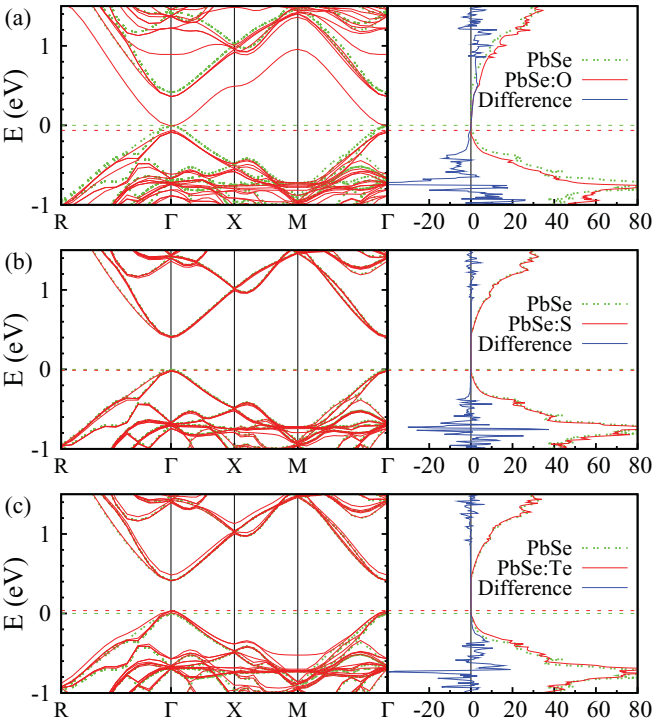

FIG. 18. (Color online) The same as in Fig. 2 but for (a) PbSe:O, (b) PbSe:S, and (c) PbSe:Te.

pulled down, and Te is less electronegative than Se, so its bands shift slightly upward. The band structure of S-doped samples are almost the same as the pure host, but from the change of the DOS we can still find that the bands are very slightly pulled downward by the negative impurity potential.

We calculated the transport properties for all three samples, and the host PbSe is used as reference. With n-type doping (which here means shifting E_F into the conduction band), PbSe:S and PbSe:Te have very similar behavior to the host sample; with p-type doping, all three samples have a similar performance to the host material, especially PbSe:S, as suggested by its band structure. The power factor of PbSe:Te is even a little bigger than that of PbSe when the carrier density is very low. This could partially explain the success of PbTe-, PbSe-, and PbS-based quantum structures in thermoelectric applications.

PbSe:O is of special interest in this study, because in a recent theoretical study,[7] replacing Se with O (the so-called "highly mismatched isoelectronic doping") is proposed to improve the power factor of ZnSe. According to the definition,[7] PbSe:O is also a "highly mismatched alloy" (HMA) like ZnSe:O, because O is isovalent with Se but much more electronegative. As shown in Fig. 19(a), we know that because of the much lower O-s, the impurity-related Pb_1-p states shift down, forming an impurity state which is almost detached from the conduction band. This is actually quite analogous to what happens in PbSe:Tl, where the impurity band is derived from the host valence band.

In Figs. 19(b)–19(d), we compare the Seebeck coefficients and electrical conductivities of n-type PbSe:O and PbSe. We did not find an enhancement of the thermoelectric properties, unlike in ZnSe:O. This means that the HMA method is not universal as a means to improve the thermoelectric properties. The main difference between ZnSe and PbSe is that the valence electrons are s electrons for Zn and p electrons for Pb. In ZnSe, the DOS has a long tail above the CBM due to a significant contribution from the Zn-s orbitals, while in PbSe, only the Se-s orbitals slightly contribute to the conduction band near the CBM. Thus, the bandwidth of the conduction band in ZnSe is much wider than that of the PbSe conduction band because of the strong s-characteristics. According to Vogl's theory,[41] if the defect potential exceeds a threshold which is in proportion to the band broadening, a state can be pulled from the conduction band; otherwise the impurity state will resonate inside the host conduction band. Hence, the similar defect potential results in a strong resonance in ZnSe:O, but a deep defect state in PbSe:O.

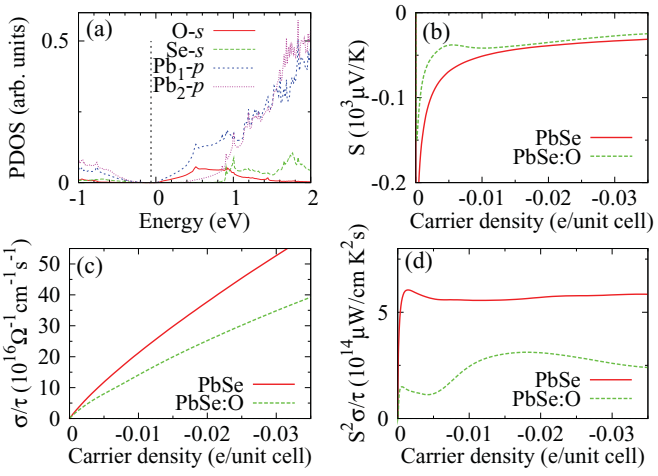

FIG. 19. (Color online) The same as in Fig. 17, but (a) for PbSe:O, (b)–(d) for PbSe:O, and the reference sample PbSe host.

IV. CONCLUSION

In this study, we calculated the band structures, density of states (DOS), change in DOS, Seebeck coefficients, electrical conductivities, and power factors of PbSe doped with various impurities. From our results and previous investigations, we conclude the following:

(i) The effects of the same impurity in PbSe and PbTe are very similar.

(ii) Impurity-p or -d orbitals are much more efficient than impurity-s orbitals to resonate with or to perturb the host bands. They are also more efficient to produce a local increase of the DOS. The former impurities include As, Sb, and Bi doped on the cation site, P, As, and Sb doped on the anion site, and Cu, Ag, and Au doped on the cation site. The latter impurities include Zn, Cd, and Hg doped on the cation site.

(iii) The impurity states near E_F in PbSe doped with Ga, In, and Tl are host states perturbed by the deep impurity-s states. We did not find an enhancement of the power factor in PbSe:Tl.

(iv) We did not find an enhancement of the power factor in PbSe:O. The highly mismatched isoelectronic doping method is not a good method to enhance the power factor of PbSe. PbSe is a kind of "5e" compound because Pb and Se have an average of five valence electrons, whereas ZnSe is a kind of "4e" compound.[30] We believe that the highly mismatched isoelectronic doping method may be good for the 4e compounds but not for the 5e compounds.

(v) PbSe:Au is a good candidate for p-type thermoelectric materials because of resonance states and a local increase of the DOS, compared with PbSe:Na.

(vi) PbSe:As_c is very likely to be a good candidate for n-type thermoelectric materials because of resonance states and a local increase of the DOS, compared with PbSe:I; further, PbSe:Zn and PbSe:Cd may be good candidates for n-type thermoelectric materials because of an additional energy pocket. But for all the n-type samples, more delicate investigations are needed because of the neglect of spin-orbit coupling in this study.

ACKNOWLEDGMENTS

We thank Vinayak Dravid for useful discussions. This work was supported by the Office of Naval Research (ONR-N-00014-09-1-0733).

APPENDIX

TABLE I. Atomic eigenvalues of valence and semicore electrons of free atom for all the elements involved in this research, which are calculated with a fully relativistic atomic program. N is the principle quantum number, κ is the usual relativistic quantum number, l and j are the orbital angular momentum and total angular momentum, and ϵ is the atomic eigenvalue.

	N	κ	l	j	ϵ (Ry)
Na					
	2	1	1	0.5	−2.129932
	2	−2	1	1.5	−2.116776
	3	−1	0	0.5	−0.213299
K					
	3	1	1	0.5	−1.402188
	3	−2	1	1.5	−1.382275
	4	−1	0	0.5	−0.184256
Rb					
	4	1	1	0.5	−1.227739
	4	−2	1	1.5	−1.161810
	5	−1	0	0.5	−0.179446
Mg					
	2	1	1	0.5	−3.449836
	2	−2	1	1.5	−3.428647
	3	−1	0	0.5	−0.358110
Ca					
	3	1	1	0.5	−2.079684
	3	−2	1	1.5	−2.051114
	4	−1	0	0.5	−0.290472
Sr					
	4	1	1	0.5	−1.743217
	4	−2	1	1.5	−1.656441
	5	−1	0	0.5	−0.274004
Cu					
	3	2	2	1.5	−0.408969
	3	−3	2	2.5	−0.389024
	4	−1	0	0.5	−0.364142
Ag					
	4	2	2	1.5	−0.593786
	4	−3	2	2.5	−0.552648
	5	−1	0	0.5	−0.353408
Au					
	5	2	2	1.5	−0.600008
	5	−3	2	2.5	−0.487146
	6	−1	0	0.5	−0.455352
Zn					
	3	2	2	1.5	−0.786489
	3	−3	2	2.5	−0.760174
	4	−1	0	0.5	−0.464021
Cd					
	4	2	2	1.5	−0.910485
	4	−3	2	2.5	−0.859025
	5	−1	0	0.5	−0.444578
Hg					
	5	2	2	1.5	−0.829684
	5	−3	2	2.5	−0.693919
	6	−1	0	0.5	−0.531628
Ga					
	4	−1	0	0.5	−0.676651
	4	1	1	0.5	−0.210649
In					
	5	−1	0	0.5	−0.621025
	5	1	1	0.5	−0.214360
Tl					
	6	−1	0	0.5	−0.697316
	6	1	1	0.5	−0.232072
Ge					
	4	−1	0	0.5	−0.876629
	4	1	1	0.5	−0.308063
Sn					
	5	−1	0	0.5	−0.783583
	5	1	1	0.5	−0.301602
Pb					
	6	−1	0	0.5	−0.851766
	6	1	1	0.5	−0.317029
P					
	3	−1	0	0.5	−1.035431
	3	1	1	0.5	−0.419798
	3	−2	1	1.5	−0.415750
As					
	4	−1	0	0.5	−1.080416
	4	1	1	0.5	−0.408706
	4	−2	1	1.5	−0.388083
Sb					
	5	−1	0	0.5	−0.954449
	5	1	1	0.5	−0.395825
	5	−2	1	1.5	−0.349972
Bi					
	6	−1	0	0.5	−1.044129
	6	1	1	0.5	−0.432079
	6	−2	1	1.5	−0.292904
O					
	2	−1	0	0.5	−1.751157
	2	1	1	0.5	−0.683374
	2	−2	1	1.5	−0.680672
S					
	3	−1	0	0.5	−1.275401
	3	1	1	0.5	−0.532349
	3	−2	1	1.5	−0.526038
Se					
	4	−1	0	0.5	−1.286509
	4	1	1	0.5	−0.511647
	4	−2	1	1.5	−0.483317
Te					
	5	−1	0	0.5	−1.125065
	5	1	1	0.5	−0.490629
	5	−2	1	1.5	−0.430780
I					
	5	−1	0	0.5	−1.297483
	5	1	1	0.5	−0.587519
	5	−2	1	1.5	−0.511932

*haowei-peng@northwestern.edu

[1] L. E. Bell, Science **321**, 1457 (2008).

[2] G. J. Snyder and E. S. Toberer, Nature Mater. **7**, 105 (2008), and references therein.

[3] J. R. Sootsman, D. Y. Chung, and M. G. Kanatzidis, Angew. Chem., Int. Ed. Engl. **48**, 8618 (2009), and references therein.

[4] G. A. Slack, in *CRC Handbook of Thermoelectrics*, edited by D. M. Rowe (Chemical Rubber, Boca Raton, FL, 1995), Chap. 34.

[5] C. M. Bhandari and D. M. Rowe, in *CRC Handbook of Thermoelectrics*, edited by D. M. Rowe (CRC, Cleveland, 1995), Chap. 5, and references therein.

[6] G. D. Mahan and J. O. Sofo, Proc. Natl. Acad. Sci. USA **93**, 7436 (1996).

[7] J.-H. Lee, J. Wu, and J. C. Grossman, Phys. Rev. Lett. **104**, 016602 (2010).

[8] J. P. Heremans, V. Jovovic, E. S. Toberer, A. Saramat, K. Kurosaki, A. Charoenphakdee, S. Yamanaka, and G. J. Snyder, Science **321**, 554 (2008).

[9] V. Fano, in *CRC Handbook of Thermoelectrics*, edited by D. M. Rowe (Chemical Rubber, Boca Raton, FL, 1995), Chap. 21, and references therein.

[10] E. A. Skrabek and D. S. Trimmer, in *CRC Handbook of Thermoelectrics*, edited by D. M. Rowe (Chemical Rubber, Boca Raton, FL, 1995), Chap. 22, and references therein.

[11] A. A. El-Sharkawy, A. M. Abou El-Azm, M. I. Kenawy, A. S. Hillal, and H. M. Abu-Basha, Int. J. Thermophys. **4**, 261 (1983).

[12] T. C. Harman and I. Meingailis, Appl. Solid State Sci. **4**, 1 (1974).

[13] S. Ahmad, S. D. Mahanti, K. Hoang, and M. G. Kanatzidis, Phys. Rev. B **74**, 155205 (2006).

[14] J. M. Ziman, *Electrons and Phonons: The Theory of Transport Phenomena in Solids* (Clarendon Press, Oxford, 1960).

[15] J. P. Perdew, K. Burke, and M. Ernzerhof, Phys. Rev. Lett. **77**, 3865 (1996).

[16] P. E. Blöchl, Phys. Rev. B **50**, 17953 (1994).

[17] G. Kresse and D. Joubert, Phys. Rev. B **59**, 1758 (1999).

[18] G. Kresse and J. Hafner, Phys. Rev. B **47**, 558 (1993); **49**, 14251 (1994).

[19] G. Kresse and J. Furthmüller, Phys. Rev. B **54**, 11169 (1996); Comput. Mater. Sci. **6**, 15 (1996).

[20] F. D. Murnaghan, Proc. Natl. Acad. Sci. USA **30**, 244 (1944).

[21] H. J. Monkhorst and J. D. Pack, Phys. Rev. B **13**, 5188 (1976).

[22] G. K. H. Madsen and D. J. Singh, Comput. Phys. Commun. **175**, 67 (2006).

[23] Yu. I. Ravich, B. A. Efimova, and V. I. Tamarchenko, Phys. Status Solidi B **43**, 11 (1971).

[24] D. I. Blic, S. D. Mahanti, and M. G. Kanatzidis, Phys. Rev. B **74**, 125202 (2006).

[25] R. Asahi, W. Mannstadt, and A. J. Freeman, Phys. Rev. B **59**, 7486 (1999).

[26] E. Wimmer, H. Krakauer, M. Weinert, and A. J. Freeman, Phys. Rev. B **24**, 864 (1981); M. Weinert, E. Wimmer, and A. J. Freeman, *ibid*. **26**, 4571 (1982).

[27] S.-H. Wei and A. Zunger, Phys. Rev. B **55**, 13605 (1997).

[28] E. A. Albanesi, C. M. I. Okoye, C. O. Rodriguez, E. L. Peltzer y Blanca, and A. G. Petukhov, Phys. Rev. B **61**, 16589 (2000).

[29] K. Hummer, A. Grüneis, and G. Kresse, Phys. Rev. B **75**, 195211 (2007).

[30] H. M. Polatoglou, Phys. Scr. **39**, 251 (1989).

[31] G. Nimtz and B. Schlicht, *Narrow-Gap Semiconductors* (Springer-Verlag, New York, 1985).

[32] A. A. Andreev, J. Phys. C **4**, 50 (1968).

[33] K. Hoang and S. D. Mahanti, Phys. Rev. B **78**, 085111 (2008).

[34] S. Ahmad, K. Hoang, and S. D. Mahanti, Phys. Rev. Lett. **96**, 056403 (2006).

[35] V. I. Kaĭdanov and Yu I. Ravich, Sov. Phys. **28**, 1 (1985), and references therein.

[36] S. A. Nemov and Yu. I. Ravich, Phys. Usp. **41**, 8 (1998), and references therein.

[37] J. Hafner, J. Comput. Chem. **29**, 2044 (2008).

[38] S. Lany and A. Zunger, Phys. Rev. B **72**, 035215 (2005).

[39] J. Androulakis and M. G. Kanatzidis (unpublished).

[40] S.-H. Wei and S. B. Zhang, Phys. Rev. B **66**, 155211 (2002).

[41] H. P. Hjalmarson, P. Vogl, D. J. Wolford, and J. D. Dow, Phys. Rev. Lett. **44**, 810 (1980); P. Vogl, Adv. Electron. Electron Phys. **62**, 101 (1984).